analytical chemistry

Technical Note

pubs.acs.org/ac

Fast Fluorescence-Based Microfluidic Method for Measuring Minimum Miscibility Pressure of CO_2 in Crude Oils

Phong Nguyen,[†] Danyal Mohaddes,[†] Jason Riordon,[†] Hossein Fadaei,[†] Pushan Lele,[†] and David Sinton*[,†]

[†]Department of Mechanical and Industrial Engineering, University of Toronto, 5 King's College Road, Toronto, Ontario M5S 3G8, Canada

Supporting Information

ABSTRACT: Carbon capture, storage, and utilization has emerged as an essential technology for near-term CO_2 emission control. The largest CO_2 projects globally combine storage and oil recovery. The efficiency of this process relies critically on the miscibility of CO_2 in crude oils at reservoir conditions. We present a microfluidic approach to quantify the minimum miscibility pressure (MMP) that leverages the inherent fluorescence of crude oils, is faster than conventional technologies, and provides quantitative, operator-independent measurements. To validate the approach, synthetic oil mixtures of known composition (pentane, hexadecane) are tested and MMP values are compared to reported values. Results differ by less than 0.5 MPa on average, in contrast to comparison between conventional methods with variations on the order of 1−2 MPa. In terms of speed, a pressure scan for a single MMP measurement required less than 30 min (with potential to be sub-10 min), in stark contrast to days or weeks with existing approaches. The method is applied to determine the MMP for Pennsylvania, West Texas, and Saudi crudes. Importantly, our fluorescence-based approach enables rapid, automated, operator-independent measurement of MMP as needed to inform the world's largest CO_2 projects.

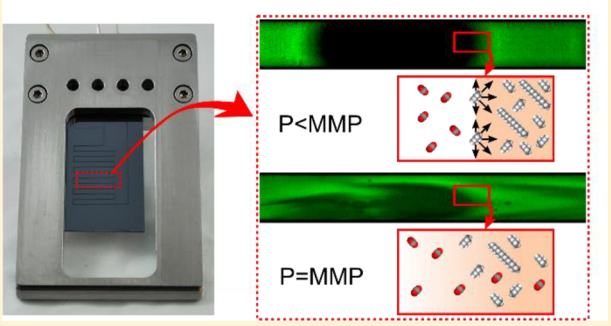

Global energy consumption has led to an increase in CO_2 emissions with climate implications.[1] Carbon capture, utilization, and storage technologies target the reduction of CO_2 emissions and sustainable global economic development.[2−4] Recent research has focused on developing effective methods of carbon capture,[5−7] CO_2 conversion to fuels,[8,9] sequestration in underground saline aquifers, and combined storage/utilization of CO_2 in enhanced oil recovery (EOR).[10,11] Currently, CO_2 EOR is the most economically and technically feasible approach (Figure 1a).[11] The majority of current CO_2 EOR projects are in North America (~120 projects).[12] The total world storage potential in enhanced oil recovery reservoirs is estimated to be 370 gigatonnes, and recoverable oil with this technology is 1.3 trillion barrels.[11]

A key parameter in CO_2 EOR is the minimum miscibility pressure (MMP) of the injected CO_2 and oil.[13] The lowest pressure at which a gas can develop miscibility through a multiple contact process with oil at a given reservoir temperature, as commonly described on the ternary phase diagram of CO_2 and oil (Figure 1b), is defined as MMP.[14] At pressures below MMP, the main driving force of mass transfer at the interface between CO_2 and oil is diffusion, which is mitigated by interfacial tension (Figure 1c). At MMP, the interfacial tension between CO_2 and oil vanishes as CO_2 vaporizes the light components of the oil to create an enriched mixture which further becomes enriched with heavier oil components, eventually becoming fully miscible with the oil (Figure 1d). Injecting CO_2 at or above MMP increases both the uptake of CO_2 in the reservoir and oil production as interfacial force barriers are eliminated and the oil is displaced as a single phase liquid.[13,15−17] Current methods used to measure the MMP of gas and oil include the rising bubble apparatus (RBA),[18] slim-tube test,[19] and vanishing interfacial tension method.[20,21] The RBA method is illustrated in Figure 1e. These current methods suffer from long measurement times (days, weeks) and/or measurement subjectivity (operator-dependent). Motivated by the cost of current experimental approaches, simulation-based methods for MMP determination have been developed.[22−25] Simulations can be comparatively inexpensive and fast. The full composition of the test oil is required, however, and simulation results can have significant error.[26] In general, simulations are best paired or fit with select experimental data.

Recently, there have been a number of new applications of microfluidics to CO_2 storage and oil recovery applications.[27] In addition to the traditional benefits of microfluidic systems (speed, small volumes, rapid diffusive transport, multiplexing), subsurface CO_2, oil and gas applications benefit from (i) high temperature and pressure tolerance of silicon/glass, and (ii) a match between microfluidic channels and microporous media typical of reservoirs.[28−39] While no microfluidic method for

Received: December 22, 2014
Accepted: February 10, 2015
Published: February 10, 2015

DOI: 10.1021/ac5047856
Anal. Chem. 2015, 87, 3160−3164

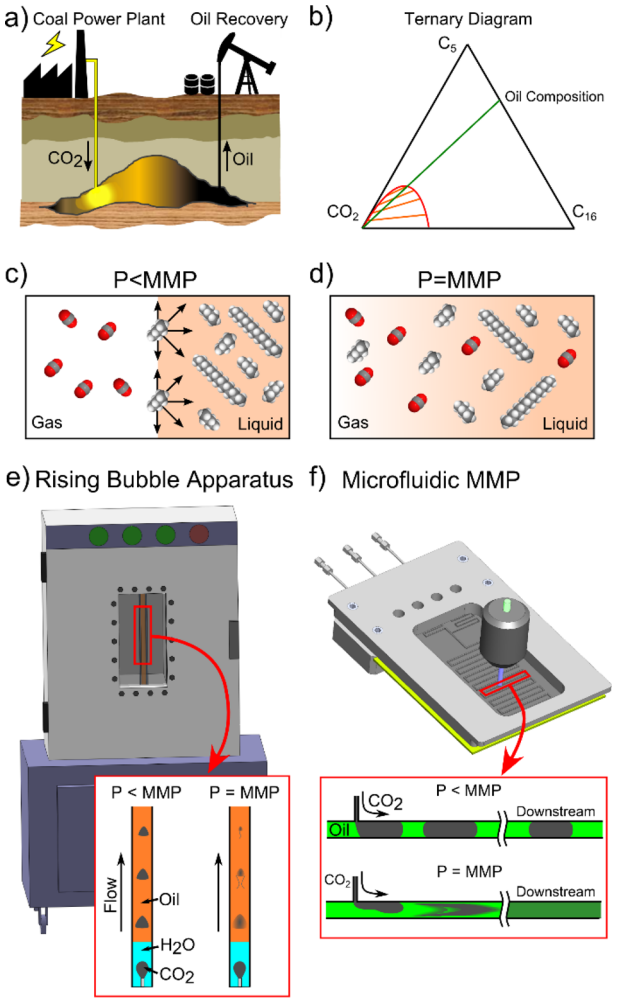

Figure 1. (a) CO_2 storage and enhanced oil recovery, CO_2 EOR. (b) Ternary diagram of CO_2 and model synthetic crude oil components (pentane and hexadecane). Molecular behavior at the oil/CO_2 interface presented at pressures (c) below MMP and (d) at MMP. (e) The conventional rising bubble apparatus (RBA) method is compared to (f) the microfluidic MMP method, each inset with corresponding bubble behaviors at pressures below and at MMP.

MMP measurement has been developed to date, both bubble generation[40−48] and droplet-based microreactors[49−59] are relevant to this approach. These microfluidic platforms have been extensively applied in lab-on-chip technology, chemical synthesis, and phase behavior studies.

Herein, we report a rapid, user-independent method for measuring CO_2-in-oil MMP at reservoir-relevant temperatures and pressures. The mixing of continuously generated CO_2 bubbles within a microchannel embedded in silicon are observed quantitatively, leveraging the inherent fluorescence of crude oil sample (Figure 1f). To validate and benchmark the method, a set of synthetic oil mixtures with known compositions of pentane and hexadecane are tested with results compared to those from the RBA method. The dependence of MMP on temperature and density (API gravity) is also demonstrated. To demonstrate wide applicability, the method is applied to measure the MMP of relevant crude oils: Pennsylvania, West Texas, and Saudi crudes.

EXPERIMENTAL METHOD

The microfluidic chip was fabricated through deep reactive ion etching of silicon, and subsequent anodic bonding to glass. Hybrid silicon-glass chips can withstand a high range of pressures and temperatures ($P \leq 40$ MPa, $T \leq 200$ °C),[60] sufficient for all practical CO_2 EOR applications. The chip design consists of a T-junction with a main channel width of 250 μm and a CO_2 nozzle width of 50 μm. Both the CO_2 and oil channels have resistors upstream of the T-junction to dampen pressure fluctuations, and all channels have a depth of 100 μm. The chip was installed on a stainless steel manifold with high pressure compression fittings (Swagelok) to provide high pressure connections to the fluid lines as shown in Figure S1 of the Supporting Information. High pressure pumps (Teledyne Incommode 260D) were used to pump CO_2 into the chip and to set the reference pressure on the backpressure regulator (Equilibar model EB1ULF1-SS316). A third high pressure pump (Eldex, Optos Series 1SMP) was used to flow oil into the chip, and the backpressure regulator was used to set the system pressure. A 60W tape heater was attached to the back of the chip to provide a set temperature on the chip. The heating tape was controlled by a temperature controller (Omega model CNi3222) within ±1 °C. A fluorescent microscope (Leica DMLM) was used to image the bubble formation and CO_2/oil phases in the chip with a 10× objective and a Semrock BrightLine filter cube (Ex 375−400, Em LP405). The images were captured with a high speed camera (model PCO 1200s) at a frame rate of 100 frames per second. The recorded images were processed in ImageJ to perform image calibration and intensity analysis. Image calibration for background removal was performed using dark and bright image based on a shading correction method given by Wilkinson et al.[61] Materials used in this work are presented in Figure S2 of the Supporting Information.

For each data set, the main channel was filled with oil to the pressure set by the backpressure regulator. Subsequently, CO_2 was injected into the oil channel from the smaller T-junction side channel (Figure 1f). The pressure was then incrementally increased, and the fluid mixing properties at the T-junction and downstream were monitored via fluorescence microscopy. In the case of synthetic oil tests, fluorescent dye (Dye-Lite, Tracerline) was added to the oil mixture at a concentration of 50 ppm to enable fluorescent imaging. In the case of crude oils, no dye was added as the inherent fluorescence was used. Between experiments, the chip was cleaned with successive flushing of toluene and acetone. In this work, we performed a vaporizing gas drive by introducing pure CO_2 into fresh oil. Although not the focus here, our microfluidic technique could in principle be expanded to measure the MMP of alternate gases, such as enriched CO_2 mixtures which are used in condensing gas drives.

RESULTS AND DISCUSSION

Figure 2a shows the changes in bubble shape with pressures below, at, and above MMP, as observed in the microfluidic chip (see also video in the Supporting Information). Below MMP, the interfacial tension between the CO_2 and oil is high, which allowed the bubbles to retain their shape with sharp channel-blocking interfaces as shown for the case of $P = 5.9$ MPa. In this regime, the mass transfer between the CO_2 phase to the oil phase is through diffusion across the interface. As a result, the CO_2 bubbles shrink as they flow downstream, as is familiar in

DOI: 10.1021/ac5047856
Anal. Chem. 2015, 87, 3160−3164

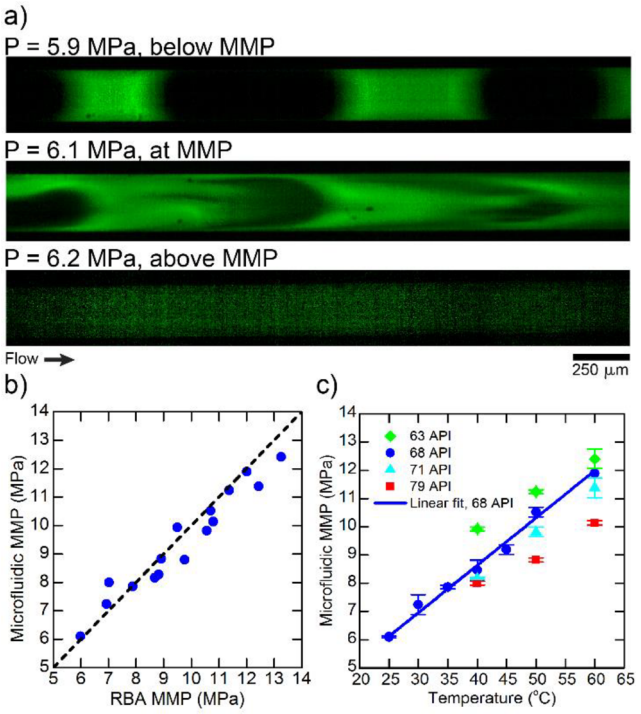

Figure 2. (a) Demonstration of high-contrast fluorescence imaging of CO_2 bubbles flowing through synthetic oil at pressures below, at, and above MMP. (b) Cross plot comparing microfluidic MMP measurements to literature MMP values from the RBA method. The 45° dashed line represents the ideal perfect correlation case. (c) Demonstration of the linear dependence of MMP on temperature for various synthetic oil mixtures (63 API, 68 API, 71 API, and 79 API). MMP increases with oil density from light to heavy oil. (A video is provided in the Supporting Information).

gas–liquid droplet reactors. As the pressure was increased to MMP (P = 6.1 MPa), the interfacial tension decreased and the injected CO_2 bubbles deformed readily in response to flow-induced stresses. Specifically, round nose-shaped bubbles were formed with trailing boundaries that were rapidly eroded as they mixed with the continuous oil phase, unimpeded by interfacial tension. Likewise, the bubble shape shown (P = 6.1 MPa) is reminiscent of miscible band broadening in Poiseuille flow,[62] and also characteristic of the shape observed in RBA at MMP.[18] Above MMP (P = 6.2 MPa), mixing is rapid, and the two phases are largely indistinguishable at the downstream location shown in Figure 2a. At the injector, distinct phases are observed at pressures moderately above MMP, and progressively less so as interfacial tension vanishes with increasing pressure.

The microfluidic method was validated by comparing measured MMP values to those measured with the RBA method.[18] These validation tests were conducted with various synthetic oil mixtures (hexadecane/pentane, 63 to 79 API) at different temperatures (25 to 60 °C). As shown in Figure 2b, MMP measurements demonstrated strong agreement with reported RBA measurements, with an average difference of 0.5 MPa. This degree of agreement is significant in the context of comparisons among MMP methods: previously reported MMP measurements using RBA and slim tube methods differ on average by 0.86 MPa,[12,18,19] and MMP measurements with vanishing interfacial tension and slim tube methods differ by 2.2 MPa.[63] Figure 2c plots the temperature-dependence for MMP measurements for synthetic oils of different density. The linear fit for 68 API has a slope of 0.168 MPa/°C, which compares well to the 0.188 MPa/°C as measured by the RBA method for this synthetic oil mixture.[19] The method was applied to other synthetic oil mixtures (63 API, 71 API, and 79 API), each providing a distinct MMP, increasing with temperature.

The method was applied to measure MMP of crude oils from large EOR candidate reservoirs worldwide. The MMP measured for Pennsylvania crude (8.34 ± 0.07 MPa) and West Texas crude (10.0 ± 0.3 MPa) at 40 °C compare well to literature data of 7.3 MPa (estimated based on Cronquist correlation)[64] and 9.7 MPa (measured with slim tube),[65] respectively (Table 1). Figure 3 illustrates how the fluidic

Table 1. Crude Oil MMP measurements

oil type	density (°API)	temperature (°C)	microfluidic MMP (MPa)
Pennsylvania	48.8	25	5.52 ± 0.07
		40	8.34 ± 0.07
West Texas	38.9	25	7.4 ± 0.2
		40	10.0 ± 0.3
Saudi Berri	37.0	25	8.3 ± 0.7
		40	10.7 ± 0.3

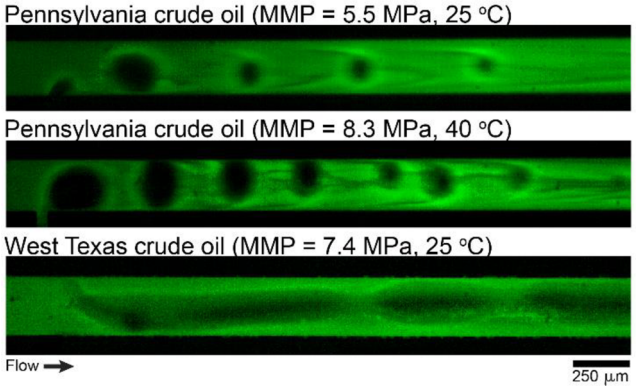

Figure 3. Microfluidic fluorescent visualization of West Texas and Pennsylvania crude oil at MMP, at 25 and 40 °C, as indicated. Each crude exhibiting a characteristic mixing pattern due to differences in oil compositions.

mixing behavior varies between the three different crude oils. This variation can be attributed mainly to differences in crude oil compositions.[66] Despite the natural variability in these oils, all three exhibit recognizable shifts in flow condition signaling MMP.

In contrast to all existing methods, a fluorescence-based microfluidic approach presents the opportunity for direct, user-independent, measurement of MMP. To demonstrate, fluorescence image sequences (1.45 s) were analyzed using ImageJ software, each corresponding to a given inlet pressure in the range of MMP. The average intensity over a 35 × 185 μm detection region within the channel was sampled in each frame and plotted over time (Figure 4, panels a and b). At sub-MMP values, oil and CO_2 plugs traversed the detection region in sequence, which generated a strong periodic oscillation between intensity plateaus. At higher pressures (6.07 MPa), fluid plugs quickly interweaved and mixed. On occasion, shrunken CO_2 plugs traversed the detection region, which caused a detectable dip in fluorescence signal (video in Supporting Information). Figure 4c shows how this intensity

DOI: 10.1021/ac5047856
Anal. Chem. 2015, 87, 3160–3164

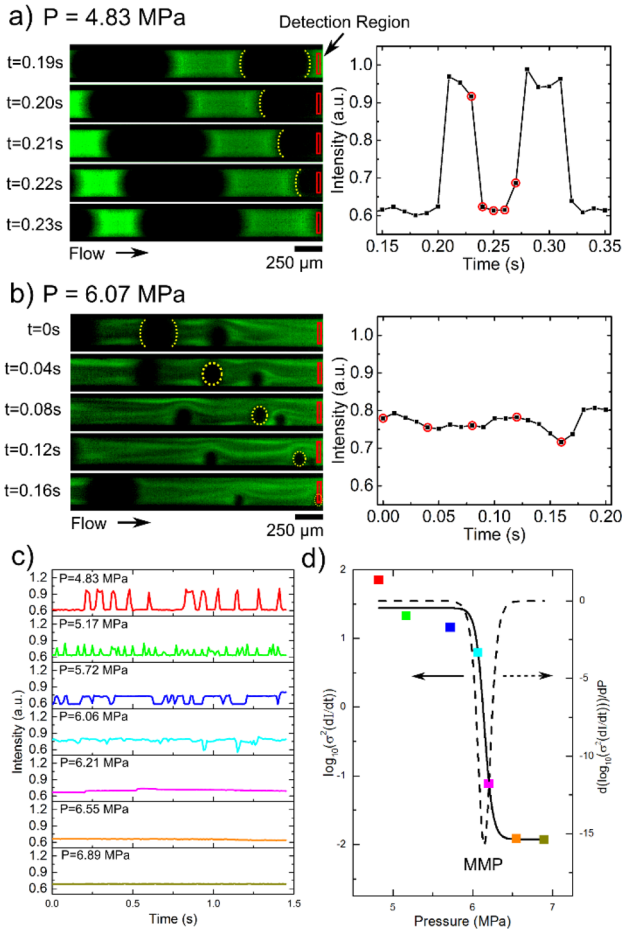

Figure 4. Operator-independent fluorescence-based measurement of MMP: fluctuations in fluorescence intensity at pressures of (a) 4.83 MPa and (b) 6.07 MPa measured over time. Data points highlighted with red circles are shown with corresponding images. (c) Variation in average intensity within the detection region over time at different pressures. The variance of the derivative of these data sets is plotted in log format in (d). The derivative of this curve is plotted to highlight the point of greatest slope, which corresponds to MMP, in this case, 6.14 MPa.

changed over time at various pressure settings, each normalized to unity. As the MMP region was approached, sharp changes in fluorescence became infrequent and eventually ceased to occur. At a pressure above MMP, the intensity signal fully stabilized. To quantify MMP directly from this data, the intensity profiles were differentiated with respect to time (Figure S3 of the Supporting Information). The variance of each of these data sets was calculated for each video segment and plotted in log format in Figure 4d. The data points were fit to the Boltzman sigmoidal equation:

$$y = \frac{A_1 - A_2}{1 + e^{(x-x_0)/dx}} + A_2$$

Fit parameters: $A_1 = 1.44 \pm 0.2$, $A_2 = -1.9 \pm 0.2$, $x_0 = 6.14 \pm 0.02$, and $dx = 0.05 \pm 0.02$. A MMP value of 6.14 MPa was determined by the inflection point, that is, the minimum of the derivative of the sigmoidal curve. This measured value compares well to the 6.1 MPa MMP value obtained by the direct visualization method.

Importantly, the curve-fit and subsequent analysis here is user-independent and requires only a few seconds. Specifically, MMP is determined from the automated fluorescence analysis, in contrast to the direct visualization used in the validation tests above. The speed of the overall method is limited only by fluid handling and pressure-stabilization. In the experiment here, ~5 min was employed for each pressure level to ensure equilibrium. Even with these conservative, long equilibrium times, quantitative MMP determination was possible in less than 30 min. With the small volume characteristic of this microfluidic system, equilibrium conditions should be achieved after one residence time (here, τ = 50 s). Thus, a single, reservoir-relevant pressure value could be obtained in ~1 min, and a pressure range sweep could be completed on the order of 5−10 min. Such timing is in stark contrast to current methods that require days to weeks and incorporate user-specific bias.

CONCLUSION

In summary, we demonstrate a microfluidic method for measuring CO_2 and oil MMP which provides two distinct advantages over conventional methods: fast measurement speed and quantitative analysis. In terms of speed, MMP can be obtained within 30 min using our microfluidic technique, compared to days or weeks using traditional methods such as RBA, slim tube, or vanishing interface methods. Further, in leveraging the inherent fluorescence of crude oils, we achieved heightened contrast between CO_2 and oil and provided the means of quantitative, user-independent, MMP measurement. Microfluidic MMP measurements were validated with the established RBA method data, showing a strong agreement with expected values under CO_2 reservoir-relevant conditions. Collectively, these results demonstrate the potential to inform and improve the largest current CO_2 operations worldwide.

ASSOCIATED CONTENT

Supporting Information

Figures of experimental setup, differential intensity variance analysis, ternary diagram of CO_2 and synthetic oil, and CO_2 mixing video. This material is available free of charge via the Internet at http://pubs.acs.org.

AUTHOR INFORMATION

Corresponding Author

*E-mail: sinton@mie.utoronto.ca.

Notes

The authors declare no competing financial interest.

ACKNOWLEDGMENTS

The authors gratefully acknowledge funding from the Natural Science and Engineering Research Council of Canada (NSERC) strategic project grant in the areas of natural resources and energy. The authors also gratefully acknowledge infrastructure funding from the Canada Foundation for Innovation (CFI).

REFERENCES

(1) Chu, S.; Majumdar, A. *Nature* **2012**, *488*, 294−303.
(2) Haszeldine, R. S. *Science* **2009**, *325*, 1647−1652.
(3) Lackner, K. S. *Science* **2003**, *300*, 1677−1678.
(4) Scott, V.; Gilfillan, S.; Markusson, N.; Chalmers, H.; Haszeldine, R. S. *Nat. Clim. Change* **2012**, *3*, 105−111.
(5) Niedermaier, I.; Bahlmann, M.; Papp, C.; Kolbeck, C.; Wei, W.; Krick Calderón, S.; Grabau, M.; Schulz, P. S.; Wasserscheid, P.; Steinrück, H.-P.; Maier, F. *J. Am. Chem. Soc.* **2014**, *136*, 436−441.

DOI: 10.1021/ac5047856
Anal. Chem. 2015, 87, 3160−3164

(6) Woodward, R. T.; Stevens, L. a; Dawson, R.; Vijayaraghavan, M.; Hasell, T.; Silverwood, I. P.; Ewing, A. V.; Ratvijitvech, T.; Exley, J. D.; Chong, S. Y.; Blanc, F.; Adams, D. J.; Kazarian, S. G.; Snape, C. E.; Drage, T. C.; Cooper, A. I. *J. Am. Chem. Soc.* **2014**, *136*, 9028−9035.
(7) Meng, L.; Burris, S.; Bui, H.; Pan, W. *Anal. Chem.* **2005**, *77*, 5947−5952.
(8) Kozak, J. a; Wu, J.; Su, X.; Simeon, F.; Hatton, T. A.; Jamison, T. F. *J. Am. Chem. Soc.* **2013**, *135*, 18497−18501.
(9) Mistry, H.; Reske, R.; Zeng, Z.; Zhao, Z.-J.; Greeley, J.; Strasser, P.; Cuenya, B. R. *J. Am. Chem. Soc.* **2014**, *136*, 16473−16476.
(10) Van Geldern, R.; Nowak, M. E.; Zimmer, M.; Szizybalski, A.; Myrttinen, A.; Barth, J. a C.; Jost, H.-J. *Anal. Chem.* **2014**, *86*, 12191−12198.
(11) Godec, M. L.; Kuuskraa, V. A.; Dipietro, P. *Energy Fuels* **2013**, *27*, 4183−4189.
(12) Dong, M.; Huang, S.; Dyer, S. B.; Mourits, F. M. *J. Pet. Sci. Eng.* **2001**, *31*, 13−22.
(13) Amao, A. M.; Siddiqui, S.; Menouar, H. SPE Improved Oil Recovery Symposium, Tulsa, OK, Apr. 14−18, 2012; Society of Petroleum Engineers: Richardson, TX; SPE-153383-MS.
(14) Wang, Y.; Orr, F. M. *J. Pet. Sci. Eng.* **2000**, *27*, 151−164.
(15) Nobakht, M.; Moghadam, S.; Gu, Y. *Ind. Eng. Chem. Res.* **2008**, *47*, 8918−8925.
(16) Abedini, A.; Mosavat, N.; Torabi, F. *Energy Technol.* **2014**, *2*, 431−439.
(17) Abedini, A.; Torabi, F. *Energy Fuels* **2014**, *28*, 774−784.
(18) Christiansen, R. L.; Haines, H. *SPE Reservoir Eng.* **1987**, 523−527.
(19) Elsharkawy, A. M.; Poettmann, F. H.; Christiansen, R. L. *Energy Fuels* **1996**, *10*, 443−449.
(20) Rao, D. N.; Lee, J. I. *J. Colloid Interface Sci.* **2003**, *262*, 474−482.
(21) Saini, D.; Rao, D. N. SPE Western Regional Meeting, Anaheim, CA, May 27−29, 2010; Society of Petroleum Engineers: Richardson, TX; SPE-132389-MS.
(22) Avaullee, L.; Trassy, L.; Neau, E.; Jaubert, J. N. *Fluid Phase Equilib.* **1997**, *139*, 155−170.
(23) Jessen, K.; Michelsen, M. L.; Stenby, E. H. *Fluid Phase Equilib.* **1998**, *153*, 251−263.
(24) Jaubert, J.-N.; Wolff, L.; Neau, E.; Avaullee, L. *Ind. Eng. Chem. Res.* **1998**, *37*, 4854−4859.
(25) Jaubert, J.-N.; Avaullee, L.; Souvay, J.-F. *J. Pet. Sci. Eng.* **2002**, *34*, 65−107.
(26) Jaubert, J.-N.; Avaullee, L.; Pierre, C. *Ind. Eng. Chem. Res.* **2002**, *41*, 303−310.
(27) Sinton, D. *Lab Chip* **2014**, *14*, 3127−3134.
(28) Schneider, M. H.; Sieben, V. J.; Kharrat, A. M.; Mostowfi, F. *Anal. Chem.* **2013**, *85*, 5153−5160.
(29) Fadaei, H.; Scarff, B.; Sinton, D. *Energy Fuels* **2011**, *25*, 4829−4835.
(30) Fadaei, H.; Shaw, J. M.; Sinton, D. *Energy Fuels* **2013**, *27*, 2042−2048.
(31) Song, W.; Fadaei, H.; Sinton, D. *Environ. Sci. Technol.* **2014**, *48*, 3567−3574.
(32) Kharrat, A. M.; Indo, K.; Mostowfi, F. *Energy Fuels* **2013**, *27*, 2452−2457.
(33) Mostowfi, F.; Molla, S.; Tabeling, P. *Lab Chip* **2012**, *12*, 4381−4387.
(34) Pinho, B.; Girardon, S.; Bazer-Bachi, F.; Bergeot, G.; Marre, S.; Aymonier, C. *Lab Chip* **2014**, *14*, 3843−3849.
(35) Nguyen, P.; Fadaei, H.; Sinton, D. *Energy Fuels* **2014**, *28*, 6221−6227.
(36) Conn, C. A.; Ma, K.; Hirasaki, G. J.; Biswal, S. L. *Lab Chip* **2014**, *14*, 3968−3977.
(37) De Haas, T. W.; Fadaei, H.; Guerrero, U.; Sinton, D. *Lab Chip* **2013**, *13*, 3832−3839.
(38) Kim, M.; Sell, A.; Sinton, D. *Lab Chip* **2013**, *13*, 2508−2518.
(39) Gunda, N. S. K.; Bera, B.; Karadimitriou, N. K.; Mitra, S. K.; Hassanizadeh, S. M. *Lab Chip* **2011**, *11*, 3785−3792.
(40) Garstecki, P.; Gitlin, I.; DiLuzio, W.; Whitesides, G. M.; Kumacheva, E.; Stone, H. a. *Appl. Phys. Lett.* **2004**, *85*, 2649.
(41) Hashimoto, M.; Whitesides, G. M. *Small* **2010**, *6*, 1051−1059.
(42) Vuong, S. M.; Anna, S. L. *Biomicrofluidics* **2012**, *6*, 022004.
(43) Stoffel, M.; Wahl, S.; Lorenceau, E.; Höhler, R.; Mercier, B.; Angelescu, D. *Phys. Rev. Lett.* **2012**, *108*, 1−5.
(44) Choi, W.; Hashimoto, M.; Ellerbee, A. K.; Chen, X.; Bishop, K. J. M.; Garstecki, P.; Stone, H. a; Whitesides, G. M. *Lab Chip* **2011**, *11*, 3970−3978.
(45) Garstecki, P.; Fuerstman, M. J.; Stone, H. a; Whitesides, G. M. *Lab Chip* **2006**, *6*, 437−446.
(46) Anna, S. L.; Bontoux, N.; Stone, H. a. *Appl. Phys. Lett.* **2003**, *82*, 364.
(47) Ahmadi, A.; Devlin, K. D.; Najjaran, H.; Holzman, J. F.; Hoorfar, M. *Lab Chip* **2010**, *10*, 1429−1435.
(48) Baret, J.-C. *Lab Chip* **2012**, *12*, 422−433.
(49) Cho, S.; Kang, D.; Sim, S.; Geier, F.; Kim, J.; Niu, X.; Edel, J. B.; Chang, S.; Wootton, R. C. R.; Elvira, K. S.; DeMello, A. J. *Anal. Chem.* **2013**, *85*, 8866−8872.
(50) Egawa, T.; Durand, J. L.; Hayden, E. Y.; Rousseau, D. L.; Yeh, S.-R. *Anal. Chem.* **2009**, *81*, 1622−1627.
(51) Najah, M.; Mayot, E.; Mahendra-Wijaya, I. P.; Griffiths, A. D.; Ladame, S.; Drevelle, A. *Anal. Chem.* **2013**, *85*, 9807−9814.
(52) Hellman, A. N.; Rau, K. R.; Yoon, H. H.; Bae, S.; Palmer, J. F.; Phillips, K. S.; Allbritton, N. L.; Venugopalan, V. *Anal. Chem.* **2007**, *79*, 4484−4492.
(53) Venancio-Marques, A.; Barbaud, F.; Baigl, D. *J. Am. Chem. Soc.* **2013**, *135*, 3218−3223.
(54) Shim, J.-U.; Cristobal, G.; Link, D. R.; Thorsen, T.; Jia, Y.; Piattelli, K.; Fraden, S. *J. Am. Chem. Soc.* **2007**, *129*, 8825−8835.
(55) Voicu, D.; Abolhasani, M.; Choueiri, R.; Lestari, G.; Seiler, C.; Menard, G.; Greener, J.; Guenther, A.; Stephan, D. W.; Kumacheva, E. *J. Am. Chem. Soc.* **2014**, *136*, 3875−3880.
(56) Wang, C.; Bains, A.; Sinton, D.; Moffitt, M. G. *Langmuir* **2013**, *29*, 8385−8394.
(57) Zhao, Y.; Shum, H. C.; Chen, H.; Adams, L. L. a; Gu, Z.; Weitz, D. a. *J. Am. Chem. Soc.* **2011**, *133*, 8790−8793.
(58) Silvera-Batista, C. A.; Weinberg, P.; Butler, J. E.; Ziegler, K. J. *J. Am. Chem. Soc.* **2009**, *131*, 12721−12728.
(59) Hashimoto, M.; Feng, J.; York, R. L.; Ellerbee, A. K.; Morrison, G.; Thomas, S. W.; Mahadevan, L.; Whitesides, G. M. *J. Am. Chem. Soc.* **2009**, *131*, 12420−12429.
(60) Marre, S.; Adamo, A.; Basak, S.; Aymonier, C.; Jensen, K. F. *Ind. Eng. Chem. Res.* **2010**, *49*, 11310−11320.
(61) Wilkinson, M. H. F. *Computer Methods and Programs in Biomedicine* **1994**, *44*, 61−67.
(62) Kirby, B. J. Micro- and nanoscale fluid mechanics: Transport in microfluidic devices, Cambridge University Press, Cambridge, 2013.
(63) Rao, D. N. *Fluid Phase Equilib.* **1997**, *139*, 311−324.
(64) Bank, G. C.; Riestenberg, D.; Koperna, G. J. SPE Eastern Regional Meeting, Lexington, KY, Oct. 17−19, 2007; Society of Petroleum Engineers: Richardson, TX; SPE-111282-MS.
(65) Shyeh-Yung, J.-G. J. SPE Annual Technical Conference and Exhibition, Dallas, TX, Oct. 6−9, 1991; Society of Petroleum Engineers: Richardson, TX; SPE-22651-MS.
(66) Lansangan, R. M.; Smith, J. L. *SPE Reservoir Eng.* **2013**, *8*, 175−182.

DOI: 10.1021/ac5047856
Anal. Chem. 2015, 87, 3160−3164